Improvement of selectivity for CO2 reduction by using Cu2ZnSnS4 electrodes modified with different buffer layers (CdS and In2S3) under visible light irradiation

Sunao Kamimura,[1,2] Yousuke Sasaki,[1] Masaki Kanaya,[1] Toshiki Tsubota,[1] and Teruhisa Ohno[1,2,3]*

[1]Department of Applied Chemistry, Faculty of Engineering, Kyushu Institute of Technology, 1-1 Sensuicho, Tobata, Kitakyushu 804-8550, Japan

[2] Research Center for Advanced Eco-fitting Technology, Kyushu Institute of Technology, 1-1 Sensuicho, Tobata, Kitakyushu 804-8550, Japan

[3] ACT-C, Japan Science and Technology Agency, 4-1-8 Honcho, Kawaguchi-shi, Saitama 322-0012, Japan

KEYWORDS: photoelectrochemical reduction of carbon dioxide, water splitting, photocathode, photocatalyst

***Corresponding author: tohno@che.kyutech.ac.jp**

ABSTRACT

The CZTS electrodes modified with different *n*-type buffer layers (CdS, In_2S_3) were used as photocathodes for CO_2 reduction under visible light irradiation ($400 < \lambda < 800$ nm) in aqueous media. Compared to bare CZTS electrode, *n*-type buffer layers (CdS, In_2S_3)-modified CZTS electrode, by which *p*−*n* heterojunction between CZTS and *n*-type buffer layers is formed, afforded a significant increase in the photocurrent assigned to CO_2 reduction. In addition, a product selectivity of CO_2 reduction was improved by surface modification with *n*-type buffer layers (CdS, In_2S_3): that is, selective CO_2 reduction into CO was achieved by using CdS/CZTS electrode, while HCOOH selectivity was observed over In_2S_3/CZTS electrode. In this paper, we investigated the photoelectrochemical properties for *n*-type buffer layers (CdS, In_2S_3)-modified CZTS electrode in conjunction with the structural and optical properties, and discuss its activity for PEC CO_2 reduction.

Introduction

Carbon dioxide (CO_2) is the thermodynamically stable product of most fossil fuel combustion process and a significant contributor to the greenhouse effect. The accumulation of CO_2 in the atmosphere has an impact on climate change and could threaten the environment and eventually the worldwide economy. The conversion of CO_2 into useful products and chemicals is thus a very attractive research area. The photoelectrochemical (PEC) reduction of CO_2 to value-added products has been widely studied as a possible technique for the mitigation of atmospheric CO_2.[1-3] Over the past few decades, tremendous work on PEC CO_2 reduction have been performed by using semiconductor electrodes in water electrolysis as both an electron donor and a proton source,[4,5] whose is currently called as an artificial photosynthesis. The one way of goal for an artificial photosynthesis is to directly convert CO_2 into organic fuels over *p*-type semiconductor electrodes (photocathodes) in combined with *n*-type semiconductor electrodes (photoanodes) for oxygen generation from water without applying an external voltage under sunlight illumination. To date, there have been many studies on high-efficiency photoanodes such as WO_3, [6,7] TaON, [8,9] Fe_2O_3,[10,11] and $BiVO_4$, [12,13] while there have been few reports on photocathodes with a high selectivity for CO_2 reduction because semiconductor electrode generally shows preferential H_2 production in the aqueous solution.

Cu_2ZnSnS_4 (CZTS) is one of the promising *p*-type semiconducting materials for PEC devices due to its ability to absorb visible light (optical band gap ca. 1.5 eV) and its relative stability in aqueous environments.[14-16] In addition, it is made of cheap, non-toxic, earth-abundant elements and can be easily produced on a large scale. The PEC CO_2 reduction utilizing CZTS electrode was first reported in 2011 by Arai *et al.*, who carried out a study where CO_2 was reduced to formate with a high selectivity (current efficiency > *ca*. 80 %) by using a Ru-complex

modified CZTS electrode under visible light irradiation ($400 < \lambda < 800$ nm).[17] In the absence of a Ru-complex, no formate was produced, indicating that active center of CO_2 reduction might be a Ru-complex. In addition, the activity for CO_2 reduction was also improved by the insertion of Se into CZTS electrode presumably due to an improvement of carrier mobility.

We inspired by their work, and interested in exploring the potential of *n*-type buffer layers (CdS, In_2S_3)-modified CZTS electrode for efficient PEC CO_2 reduction reaction. Since the deposition of *n*-type buffer layers (CdS, In_2S_3) over the *p*-type CZTS layer forms a depletion region at the solid-solid interface (*p*-n heterojunction), which could also assist in extracting photo-generated electrons from CZTS toward the *n*-type buffer layers, resulting in an enhancement of photocurrent.[18-20] Moreover, the colloidal CdS have been studied as visible light responsive photocatalysts that showed the activities for CO_2 reduction to form CO with high quantum yields from DMF involving sacrificial reagents.[21] Li *et al.* reported that In_2S_3 exhibited visible-light activity toward photocatalytic reduction of CO_2 in the presence of water vapor into renewable CH_4.[22] On the basis of these observations, enhancement of the photocurrent and improvement of selectivity for CO_2 reduction was anticipated by using *n*-type buffer layers (CdS, In_2S_3)-modified CZTS electrode. However, as far as we know, there has been no report on PEC CO_2 reduction by using of *n*-type buffer layers-modified CZTS electrode. The present research carried out from this stand point.

We fabricated CZTS electrode by sol-gel spin-coating method on molybdenum-coated glass substrate. In addition, the different *n*-type buffer layers such as CdS and In_2S_3 were deposited on CZTS electrode by chemical bath deposition (CBD) method. The bare CZTS electrode exhibited a cathodic photocurrent under visible light irradiation, and the photocurrent reached ca.−100 $\mu A/cm^2$ at 0V vs. reversible hydrogen electrode (RHE) in CO_2-saturated $NaHCO_3$ solution.

Moreover, the cathodic photocurrent was enhanced by deposition of *n*-type buffer layers due to efficient charge carrier separation as a result of the creation of a *p*−*n* heterojunction, which leading to PEC reaction with the primary product being hydrogen, carbon monoxide, and formate. In this paper, the PEC properties of CZTS electrode were investigated in conjunction with structural and optical properties, and we discuss the contributions of *n*-type buffer layers (CdS, In_2S_3) on the CO_2 reduction property.

Experimental

Preparation of Cn_2ZnSnS_4 electrode

The Cu_2ZnSnS_4 electrode was fabricated by sol-gel and spin-coating method as the following procedure.[23] The 0.4 mol/L $Cu(CH_3COO)_2 \cdot H_2O$ (Wako, 99.0 %), 0.25 mol/L $Zn(CH_3COO)_2 \cdot 2H_2O$ (Wako, 99.9 %), 0.2 mol/L $SnCl_2 \cdot 2H_2O$ (Wako, 99.9 %) and 1.6 mol/L $SC(NH_2)_2$ (Wako, 98 %) were dissolved in 2-methoxyethanol (10 mL, Wako, 99.0 %) containing monoethanolamine (Sigma-Aldrich, >99.0%). The concentration of each metal ion coincides with the generally reported data for high efficiency solar cells, meanwhile excess thiourea was used to complex metal ions and alleviate the loss of sulfur during the annealing process. To avoid cracks forming in the precursor thin film during the sulfurization process, additive monoethanolamine are necessary in the precursor solution. Approximately 70 μL of the precursor solution was dropped on the Mo-coated soda lime glass (Mo/glass, size 18 mm × 20 mm, GEOMATEC Co., Ltd.) and then the excess precursor solution was removed by spin-coating (3000 rpm, 30 s). The electrode was dried in air at 200 ^oC for 5 min on a hotplate in air. After this process had been repeated for a maximum of 5 times, the electrode was calcined in air at 560 ^oC for 1 h in sulfur/N_2 atmosphere. To remove the impurity phase such as $Cu_{2-x}S$ over the

CZTS film, $(NH_4)_2S$ etching processes were performed for 6 h. Then bare CZTS electrode was obtained.

Surface modification with n-type buffer layers

The *n*-type buffer layers (CdS, In_2S_3) were deposited on the CZTS electrode by chemical bath deposition (CBD) method as the following procedure. The CZTS electrode was immersed in 0.125 mol/L $Cd(CH_3COO)_2 \cdot 2H_2O$ (Wako, 98.0 %), 2.8 mol/L $SC(NH_2)_2$ (Wako, 98 %), and NH_3 aqueous solution at 65 °C for 9 min to yield CdS-modified CZTS (CdS/CZTS). For the In_2S_3-modified CZTS (In_2S_3/CZTS), the CZTS electrode was immersed in an aqueous solution containing 0.025 mol/L $InCl_3 \cdot 4H_2O$ (Wako, 99.9 %), 0.1 mol/L CH_3CSNH_2 (Wako, 98.0 %), and 0.1 mol/L CH_3COOH (Wako, 99.7 %) at 65 °C for 15 min. After the CBD techniques, those electrodes were annealed at 200°C and 100 °C, respectively, and then CdS/CZTS and In_2S_3/CZTS electrodes were fabricated.

Characterization

The crystalline phases were characterized by using a powder X−ray diffraction (XRD) instrument (MiniFlex II, Rigaku Co.) with CuKα (λ=1.5418 Å) radiation (cathode voltage: 30 kV, current: 15 mA). Raman spectroscopy was measured by using a JASCO NRS 5100 laser raman spectrophotometer. The absorption properties of CZTS electrode were measured using the diffuse reflection method with a UV/VIS/NIR spectrometer (V570, JASCO Co., Japan) attached to an integral sphere at room temperature. Mott-schottky analysis was carried out by using an electrochemical analyzer (604D, ALS Co.) with bare CZTS electrode, platinum electrode, Ag/AgCl electrode and 0.1 M Na_2SO_4 + NaOH solution (pH=9.5) used as a working electrode, counter electrode, reference electrode and electrolyte, respectively. X−ray

photoelectron spectroscopy (XPS) measurements were performed by using a Kratos AXIS Nova spectrometer (Shimazu Co.) with a monochromatic Al Kα X−ray source. The binding energy was calibrated by taking the carbon (C) 1s peak of contaminant carbon as a reference at 284.6 eV.

Photoelectrochemical (PEC) measurement

The PEC performance of CZTS electrode was investigated in a three−electrode configuration using Ag/AgCl reference electrode and a Pt coil counter electrode. The electrolyte was CO_2-saturated 0.1 M $NaHCO_3$ solution. Linear sweep voltammetry and chronoamperometry measurements were carried out by using an automatic polarization system (HSV−110, Hokuto Denko Co.) under a Xe lamp equipped with an L−42 cut−off filter (SCF−50s−42L, SIGMAKOKI Co., Ltd.) and IR cut−off filter ($400 < \lambda < 800$ nm). The scan rate for the linear sweep voltammetry was 10 mV s^{-1}.

Analysis of products

The PEC CO_2 reduction was performed in a gastight three−electrode configuration cell with double compartment where CZTS electrode, Pt wire and silver−silver chloride (Ag/AgCl) electrodes were used as a working electrode, counter electrode and reference electrode, respectively. The electrolyte solution was 0.1 M $NaHCO_3$, which was purged with CO_2 gas for ca. 40 min prior to the start of measurement. After CO_2 bubbling, the cell was sealed and irradiated by visible light irradiation (Xe lamp, $420 \text{ nm} < \lambda < 800$ nm) for 1 h. Evolved H_2, CO gas was detected by an on−line gas chromatograph (GC) with a thermal conductivity detector (Agilent Technology Co. MicroGC) equipped with MS−5A column. He gas was used as the carrier gas. The liquid CO_2 reduction product, formic acid (HCOOH), was detected by

using single-channel ion chromatography (ICS900, Thermo Fisher Scientific Inc.), and other products including methanol (CH_3OH), ethanol (C_2H_5OH), and formaldehyde (HCOH) were detected by gas chromatography (G-3500, Hitachi Co.) with a DB-WAXetr column (122-7332, Agilent Co.).

RESULTS AND DISCUSSION

3.1. Structural and optical properties of CZTS electrode

Figure 1(a) shows the XRD pattern of CZTS electrode, together with the ICDD standard file of the tetragonal phase of Cu_2ZnSnS_4 (JCPDS 00-026-0575). An intense peak corresponding to the bottom Mo substrate was observed at 40.02°, while the other diffraction peaks were coincided with the reference pattern corresponding to (112), (200), (220), (312), (224) planes of CZTS, indicating that CZTS crystal could be synthesized by sol-gel and spin-coating method. **Figure 1(b)** shows the Raman spectrum of CZTS electrode under 532 nm laser illumination. An intense peak centered at 333 cm^{-1} along with two weak peaks located at 288 cm^{-1}, and 368 cm^{-1}; these signals are in agreement with those of the kesterite CZTS structure,[24-26] and no other peaks were found to be binary phases such as hexagonal $Cu_{2-x}S$ (475 cm^{-1}), Sn_2S_3 (304 cm^{-1}), ZnS (352 cm^{-1}) and cubic Cu_2SnS_3 (303 cm^{-1} and 356 cm^{-1}).[27] However, SnO_2 phase was observed at 663 cm^{-1}.[23] Therefore, our-fabricated CZTS electrode consists of the major phase of kesterite CZTS and the minor phases of SnO_2. Although a slightly weak peak corresponds to hexagonal MoS_2 phase was observed at 400 cm^{-1},[23,27] the MoS_2 phase plays an important role for the characteristics of CZTS electrode, as described later.

Figure 2 shows top and cross-section SEM photographs for CZTS electrode. Flat and tight structure of CZTS was observed to have good adhesion to the Mo substrate. As seen in this

photograph, a thickness of CZTS layer was estimated to be ca. 400 nm. Moreover, the MoS_2 layer was observed at an interface between CZTS layer and Mo substrate. A formation of the MoS_2 layer was inevitable via a sulfurization process of the CZTS, which may facilitate an electrical quasi-ohmic contact and improve the adhesion of CZTS to Mo back contact, but leads to high series resistance and accordingly deteriorates the device efficiency if not thin enough. In this study, we optimized the thicknesses of CZTS layer and MoS_2 layer by adjusting spin-coating and sulfurization process, respectively.

Figure 3 shows the diffuse reflectance spectrum of CZTS electrode. The CZTS is a direct energy gap material. The optical absorption of CZTS could be converted to Tauc plot, $(F(R\infty)h\nu)^n$ vs. $h\nu$, where n = 2 for a direct bandgap, by extending the tangential lines to the abscissa. The band gap estimated was ca. 1.5 eV, which is well-consistent with the reported ones in references.[28]

3.2. Structural properties of buffer layers-modified CZTS electrode

Surface modifications of the CZTS electrode with *n*-type buffer layers were performed by using the CBD method. **Figure 4** shows the top and cross-section SEM photographs for *n*-type buffer layers (CdS, In_2S_3)-modified CZTS electrodes. Compared to bare CZTS, the surface morphology was appreciably changed: the surface of CdS/CZTS electrode was composed of porous grains with sizes on the order of several micrometers. In contrast, the In_2S_3/CZTS electrode surface was composed of billowing thin layer. As seen in these cross-section SEM photographs, the thicknesses of CdS and In_2S_3 buffer layers were estimated to be ca. 50 nm and ca. 60 nm, respectively. In addition, these layers would be fabricated as β-CdS and β-In_2S_3 as confirmed by Raman spectra analysis of these layers deposited on a Mo/glass (see **Fig. 5**).[16,29-31]

Therefore, *n*-type buffer layers (CdS, In_2S_3) could be formed over CZTS electrode by CBD method.

3.2. Photoelectrochemical property of CZTS electrode

Figure 6 shows the current-potential curves for bare CZTS, CdS/CZTS and In_2S_3/CZTS electrodes in 0.1 M $NaHCO_3$ solution purged with CO_2 gas with irradiation of visible light ($400 < \lambda < 800$ nm). The bare CZTS electrode exhibited a cathodic photocurrent in response to an irradiation of incident light, and the photocurrent density reached ca. –160 $\mu A/cm^2$ at –1.0 V vs. Ag/AgCl. The cathodic photocurrent was increased by ca. 2 times after deposition of *n*-type buffer layers (CdS, In_2S_3) because of efficient charge separation at depletion region of *p*-*n* heterojunction between *p*-type CZTS and *n*-type buffer layers. Moreover, deposition of Pt contributed to further enhancement of the cathodic photocurrent due to an improvement of surface reaction rate (see **Fig. S1** in ESI); however, the observed photocurrent was attributed to water reduction reaction with the primary product being hydrogen, as will be discussed later. No CO_2 reduction products was observed in Pt/CZTS, Pt/CdS/CZTS, and Pt/In_2S_3/CZTS, thereby, we studied the PEC CO_2 reduction by using bare CZTS, CdS/CZTS and In_2S_3/CZTS electrodes hereafter.

Figure 7 shows the time courses of the cathodic photocurrent from bare CZTS, CdS/CZTS and In_2S_3/CZTS electrodes in 0.1 M $NaHCO_3$ solution purged with CO_2 gas at –1.0 V vs. Ag/AgCl under visible light irradiation ($400 < \lambda < 800$ nm). For bare CZTS electrode, the cathodic photocurrent rapidly increased when visible light was exposed, and then the photocurrent remained constant with time. The XPS spectra for Cu 2p, Zn 2p, Sn 3d and S 2p was barely changed before and after PEC measurement (see **Fig. S2** in ESI), thereby, bare CZTS

electrode is a stable upon PEC reaction. In contrast, the cathodic photocurrent for CdS/CZTS and In_2S_3/CZTS showed a slight increase up to about 20 min and was relatively stable over the observed time course. Similar tendency has been reported by Moriya *et al.* and Septina *et al.* who indicated that CdS buffer layer in Pt/CdS/$CuGaSe_2$ and Pt/CdS/Cu(In,Ga)S_2 was dissolved into electrolyte upon PEC reaction due to photocorrosion of CdS, and the cathodic photocurrent in the electrodes may have increased as the CdS buffer layer became thinner.[32,33] Indeed, we analyzed the metal cation species in the electrolyte by ICP−AES, where the Cd and In ions were detected in the electrolyte after 1 h of PEC reaction, indicating that CdS and In_2S_3 buffer layer over CZTS electrode was dissolved.

We examined PEC CO_2 reduction over bare CZTS, CdS/CZTS and In_2S_3/CZTS electrodes at –1.0 V Ag/AgCl in CO_2-saturated 0.1 M $NaHCO_3$ solution under visible light irradiation ($400 < \lambda < 800$ nm, 100 mW/cm^2). These results are shown in **Table 1**. For bare CZTS electrode, the H_2, CO and HCOOH were detected as products and no formation of CH_4, CH_3OH and C_2H_5OH was observed. The thermodynamic potential for PEC reduction of CO_2 to CO and HCOOH in the presence of protons is generally explained by the following equation:

$$CO_2 + 2H^+ + 2e^- \rightarrow HCOOH + H_2O \text{ (–0.61 V } \textit{vs.} \text{ NHE)}$$

$$CO_2 + 2H^+ + 2e^- \rightarrow CO + H_2O \text{ (–0.53 V } \textit{vs.} \text{ NHE)}$$

Here, the conduction potential of the CZTS electrode was estimated to be –1.25 V vs. RHE by Mott-Schottky analysis (see **Fig. S3** in ESI), thereby, the CO_2 reduction reactions into CO and HCOOH were thermodynamically favorable. However, the calculated faradic efficiency for H_2, CO and HCOOH was approximately 76 %, 1 % and 2 %, respectively, indicating that most of the cathodic photocurrent of bare CZTS electrode was derived from H_2 evolution. This result indicated that water reduction reaction was more preferentially caused over CZTS electrode in

the aqueous solution. In contrast, the CO evolution was increased by depositing CdS buffer layer over CZTS electrode and its faradic efficiency increased up to 7 %, implying that selectivity for CO_2 reduction was improved by using CdS/CZTS electrode. It should be noted that no CO evolution was observed when PEC measurement was performed in Ar-saturated Na_2SO_4 aqueous solution or in the dark condition, suggesting that evolved-CO gas was derived from PEC reduction of purged-CO_2 gas over CdS/CZTS electrode. In addition, Pt-modified CdS/CZTS electrode exhibited H_2 evolution with trace CO and trace HCOOH in CO_2-saturated $NaHCO_3$ aqueous solution under visible light irradiation. Taking into consideration that Pt shows high activity for H_2 evolution with a low overpotential, it is highly possible that water reduction reaction was more preferentially caused over Pt/CdS/CZTS electrode rather than CO_2 reduction. These results indicated that the CdS buffer layer plays an important role for selective PEC CO_2 reduction into CO. Indeed, Yanagida *et al.* proposed that the CO evolution over CdS nanoparticle was caused by adsorption of CO_2 molecule at CdS surface with sulfur vacancies through bidentate-type adsorption of CO_2, resulting in selective CO formation.[21] Therefore, our-observation was reasonable. On the other hands, the In_2S_3/CZTS electrode generated a relatively high HCOOH by comparison with bare CZTS electrode. Its origin is currently unknown. Li *et al.* reported that In_2S_3 contributed to visible-light activity toward photocatalytic reduction of CO_2 into CH_4 without any other products.[22] In addition, Ge *et al.* investigated the CO_2 adsorption over (110)-indium oxides by DFT calculation, where CO_2 molecule was adsorbed at In atom and oxygen vacancies through bidentate-type adsorption of CO_2.[34,35] Such CO_2 reduction process is very similar to the present reaction of CdS buffer layer, which described above. On the basis of those reports, the PEC CO_2 reduction by using In_2S_3/CZTS electrode may be occurring on the In_2S_3 surfaces and thus likely show a selective CO_2 reduction into HCOOH. Thus, *n*-type buffer

layer (CdS, In_2S_3)-modified CZTS electrode showed high photocurrent response and selectivity for CO_2 reduction, which strongly dependent on a kind of buffer layers: that is, CO selectivity was improved by deposition of CdS buffer layer, while HCOOH selectivity was improved by deposition of In_2S_3 buffer layer.

Conclusions

We fabricated CZTS electrode by sol-gel and spin-coating method on a Mo/glass substrate, and performed photoelectrochemical CO_2 reduction under visible light irradiation (λ >420 nm). The CZTS electrode exhibited a cathodic photocurrent under visible light irradiation, however its PEC reaction with the primary product being H_2 (faradaic efficiency > 76%). By depositing *n*-type buffer layer (CdS, In_2S_3) over CZTS electrode, enhancement of photocurrent response and improvement of selectivity for CO_2 reduction were achieved: that is, CO selectivity was improved by deposition of CdS buffer layer, and its faradaic efficiency was increased up to 7%. In contrast, HCOOH selectivity was improved by deposition of In_2S_3 buffer layer, and its faradaic efficiency was increased up to 5%. The improvement of selectivity for CO_2 reduction was related to a kind of *n*-type buffer layers, where the adsorption of CO_2 molecules at *n*-type buffer layers (CdS, In_2S_3) plays an important role for selective PEC CO_2 reduction. Further research is underway to test this via the deposition of surface co-catalysts that can facilitate PEC CO_2 reduction. This study could be applied to improve the selectivity for CO_2 reduction by using other Cu-chalcogenide photocathode.

ACKNOWLEDGEMENTS

The authors thank to Prof. Shigeru Ikeda of Konan University and Prof. Tetsuya Haruyama for their valuable contributions to this study. This work has been supported by a grant from Advanced Catalytic Transformation program for Carbon utilization (ACT-C), Japan Science and Technology Agency (JST).

REFERENCES

1 M. Halmann, *Nature*, 275 *(*1978) 115−116.

2 M. Schreier, P. Gao, M. T. Mayer, J. Luo, T. Moehl, M. K. Nazeeruddin, S. D. Tilley and M. Grätzel, *Energy Environ. Sci.*, 2015, **8**, 855−861.

3 G. Sahara, R. Abe, M. Higashi, T. Morikawa, K. Maeda, Y. Ueda and O. Ishitani, *Chem. Commun.*, 2015, **51**, 10722−10725.

4 S. Sato, T. Arai, T. Morikawa, K. Uemura, T. M. Suzuki, H. Tanaka and T. Kajino, *J. Am. Chem. Soc.*, 2011, **133**, 15240−15243.

5 T. Arai, S. Sato, T. Kajino and T. Morikawa, *Energy Environ. Sci.***,** 2013, **6**, 1274−1282.

6 K. Sivula, F. L. Formal and M. Grätzel, *Chem. Mater.*, 2009, **21**, 2862−2867.

7 J. A. Seabold and K. S. Choi, *Chem. Mater.*, 2011, **23**, 1105–1112.

8 M. Higashi, K. Domen and R. Abe, *Energy Environ. Sci.*, 2011, **4**, 4138−4147.

9 M. Higashi, K. Domen and R. Abe, *J. Am. Chem. Soc*., 2012, **134**, 6968−6971.

10 A. Kay, I. Cesar and M. Grätzel, *J. Am. Chem. Soc*., 2006, **128**, 15714−15721.

11 K. Sivula, R. Zboril, F. Le Formal, R. Robert, A. Weidenkaff, J. Tucek, J. Frydrych and M. Grätzel, *J. Am. Chem. Soc*., 2010, **132**, 7436−7444.

12 K. Sayama, A. Nomura, T. Arai, T. Sugita, R. Abe, M. Yanagida, T. Oi, Y. Iwasaki, Y. Abe and H. Sugihara, *J. Phys. Chem. B,* 2006, **110**, 11352−11360.

13 Y. H. Ng, A. Iwase, A. Kudo and R. Amal, *J. Phys. Chem. Lett.*, 2010, **1**, 2607−2612.

14 D. Yokoyama, T. Minegishi, K. Jimbo, T. Hisatomi, G. Ma, M. Katayama, J. Kubota, H. Katagiri and K. Domen, *Appl. Phys. Express*, 2011, **3**, 101202.

15 L. Rovelli, S. D. Tilley and K. Sivula, *ACS Appl. Mater. Interfaces,* 2013, **5**, 8018−8024.

16 F. Jiang, Gunawan, T. Harada, Y. Kuang, T. Minegishi, K. Domen and S. Ikeda, *J. Am. Chem. Soc.,* 2015, **137**, 13691−13697.

17 T. Arai, S. Tajima, S. Sato, K. Uemura, T. Morikawa and T. Kajino, *Chem. Commun.*, 2011, **47**, 12664−12666.

18 N. Guijarro, M. S. Prévot and K. Sivula, *J. Phys. Chem. Lett.*, 2014, **5**, 3902−3908.

19 P. Wang, T. Minegishi, G. Ma, K. Takanabe, Y. Satou, S. Maekawa, Y. Kobori, J. Kubota and K. Domen, *J. Am. Chem. Soc.*, 2012, **134**, 2469−2472.

20 C. Yan, F. Liu, N. Song, B. K. Ng, J. A. Stride, A. Tadich and X. Hao., *Appl. Phys. Lett*., 2014, **104**, 173901.

21 H. Fujiwara, H. Hosokawa, K. Murakoshi, Y. Wada, S. Yanagida, T. Okada, and H. Kobayashi, *J. Phys. Chem.* B 1997, **101**, 8270−8278.

22 H. Li, Y. Gao, Y. Zhou, F. Fan, Q. Han, Q. Xu, X. Wang, M. Xiao, C. Li and Z. Zou, *Nano Lett.,* **DOI:** 10.1021/acs.nanolett.6b02094

23 Z. Su, K. Sun, Z. Han, H. Cui, F. Liu, Y. Lai, J. Li, X. Hao, Y. Liu and M. A. Green, *J. Mater. Chem.* A, 2014, **2**, 500−509.

24 M. Altosaar, J. Raudoja, K. Timmo, M. Danilson, M. Grossberg, J. Krustok and E. Mellikov, *Phys. Stat. Sol. a*, 2008, **205**, 167–170.

25 P. A. Fernandes, P.M.P. Salomé, A.F. da Cunha, *Thin Solid Films*, 2009, **517**, 2519–2523.

26 K. Wang, O. Gunawan, T. Todorov, B. Shin, S. J. Chey, N. A. Bojarczuk, D. Mitzi and S. Guha, *Appl. Phys. Lett.*, 2010, **97**, 143508.

27 P.A. Fernandes, P.M.P. Salomé, A.F. da Cunha, *J. Alloys and Compounds*, 2011, **509**, 7600–7606.

28 H. Katagiri, K. Saitoh, T. Washio, H. Shinohara, T. Kurumadani and S. Miyajima, *Solar Energy Materials & Solar Cells*, 2001, **65**, 141–148.

29 I. O. Oladejia, L. Chowa, J. R. Liub, W. K. Chub, A. N. P. Bustamantec, C. Fredricksena, A. F. Schulte, *Thin Solid Films*, 2000, **359**, 154–159.

30 O. Zelaya-Angel, F. de L. Castillo-Alvarado, J. Avendailo-Lopez, A. Escamilla-Esquivel, G. Contreras-Puente, R. Lozada-Morales and G. Torres-Delgadod, *Solid State Commun.* 1997, **104**, 161–166.

31 E. Kärber, K. Otto, A. Katerski, A. Mere and M. Krunks, Mater. Sci. Semi. Proc., 2014, **25**, 137–142.

32 M. Moriya, T. Minegishi, H. Kumagai, M. Katayama, J. Kubota and K. Domen, *J. Am. Chem. Soc.*, 2013, **135**, 3733−3735.

33 W. Septina, Gunawan, S. Ikeda, T. Harada, M. Higashi, R. Abe and M. Matsumura, *J. Phys. Chem. C*, 2015, **119**, 8576−8583.

34 J. Ye, C. Liu, D. Mai and Q. Ge, *ACS Catalyst*, 2013, **3**, 1296−1306.

35 J. Ye, C. Liu and Q. Ge, *J. Phys. Chem. C*, 2012, **116**, 7817−7825.

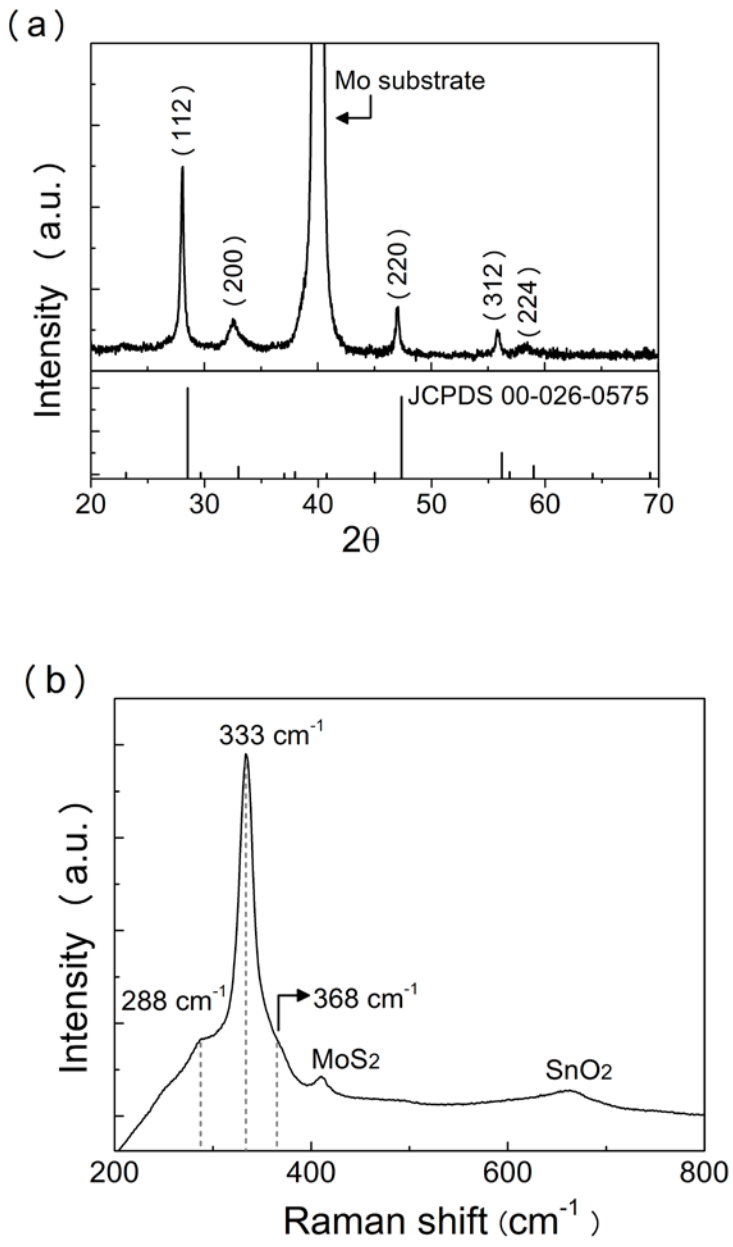

Figure 1. (a) XRD pattern of CZTS electrode, together with that of reference pattern. (b) Raman spectrum of CZTS electrode under 532 laser illumination.

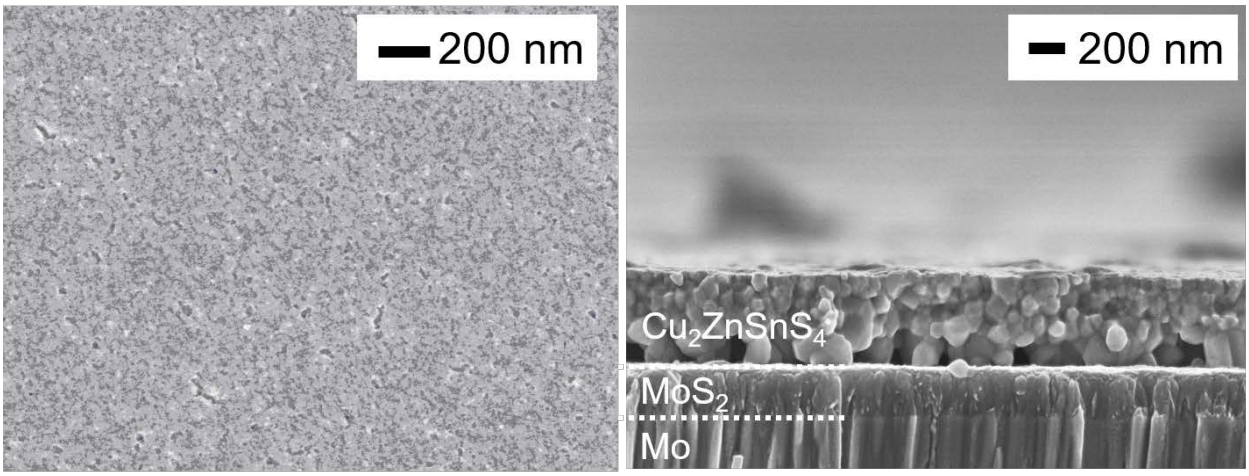

Figure 2. Top (left) and cross-sectional (right) SEM photographs of CZTS electrode.

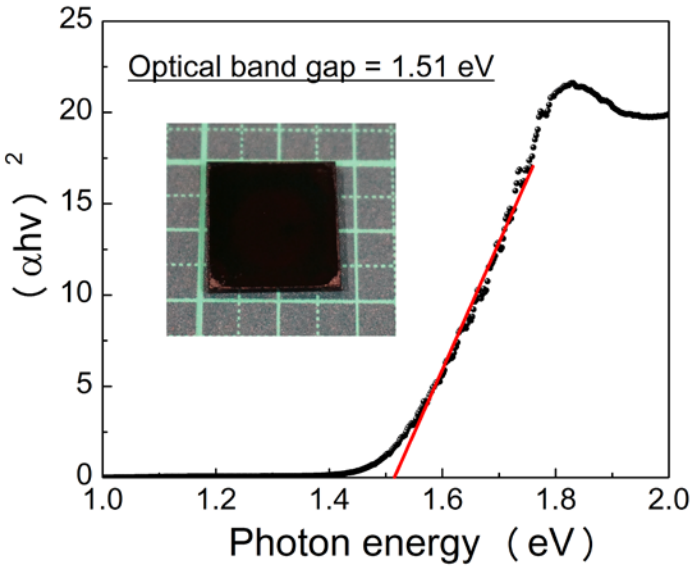

Figure 3. Tauc plot for CZTS electrode. Inset figure shows a picture for our-fabricated CZTS electrode.

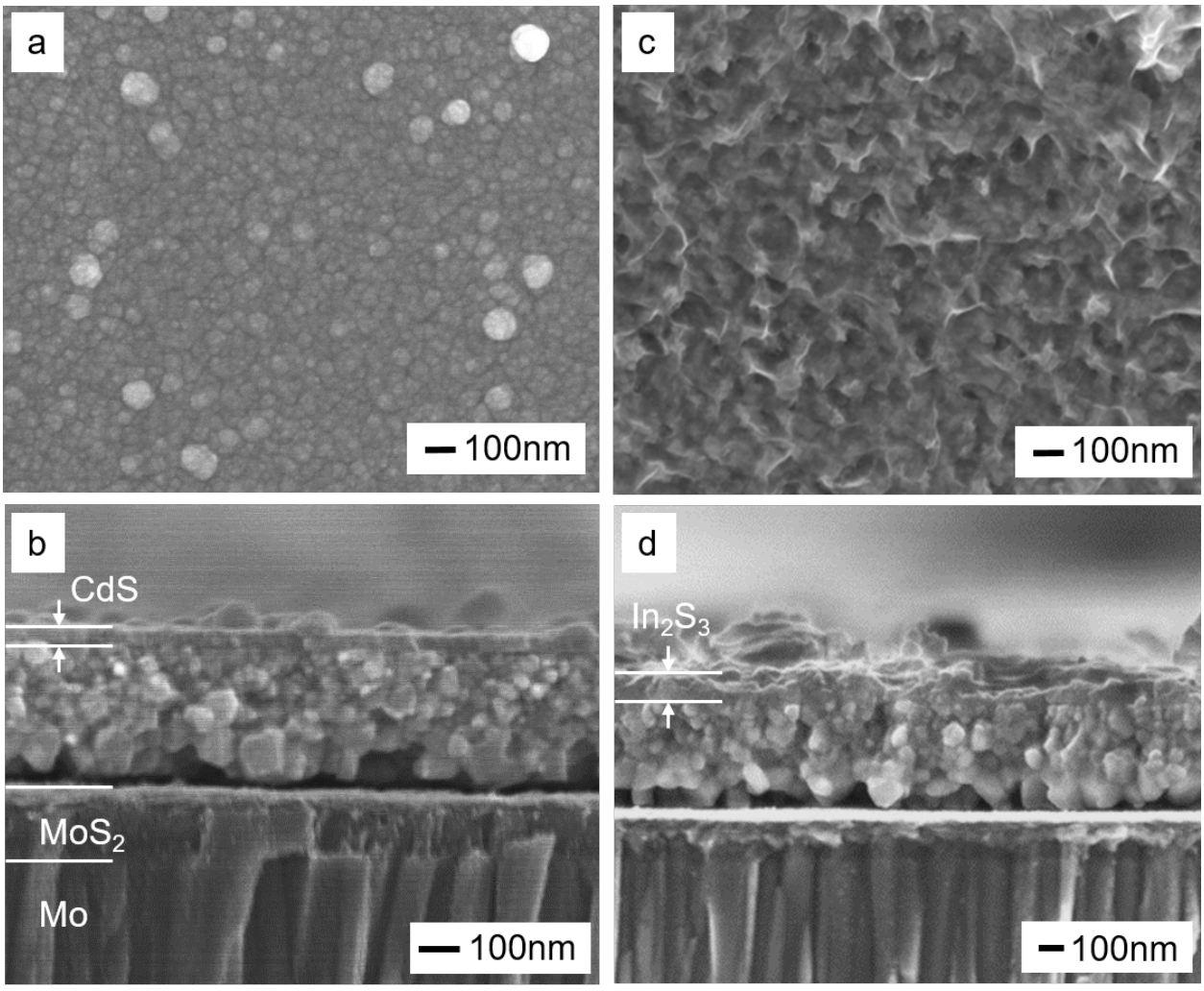

Figure 4. Top and cross-sectional SEM photographs for (a), (b) CdS/CZTS electrode, (c), (d) In_2S_3/CZTS electrode.

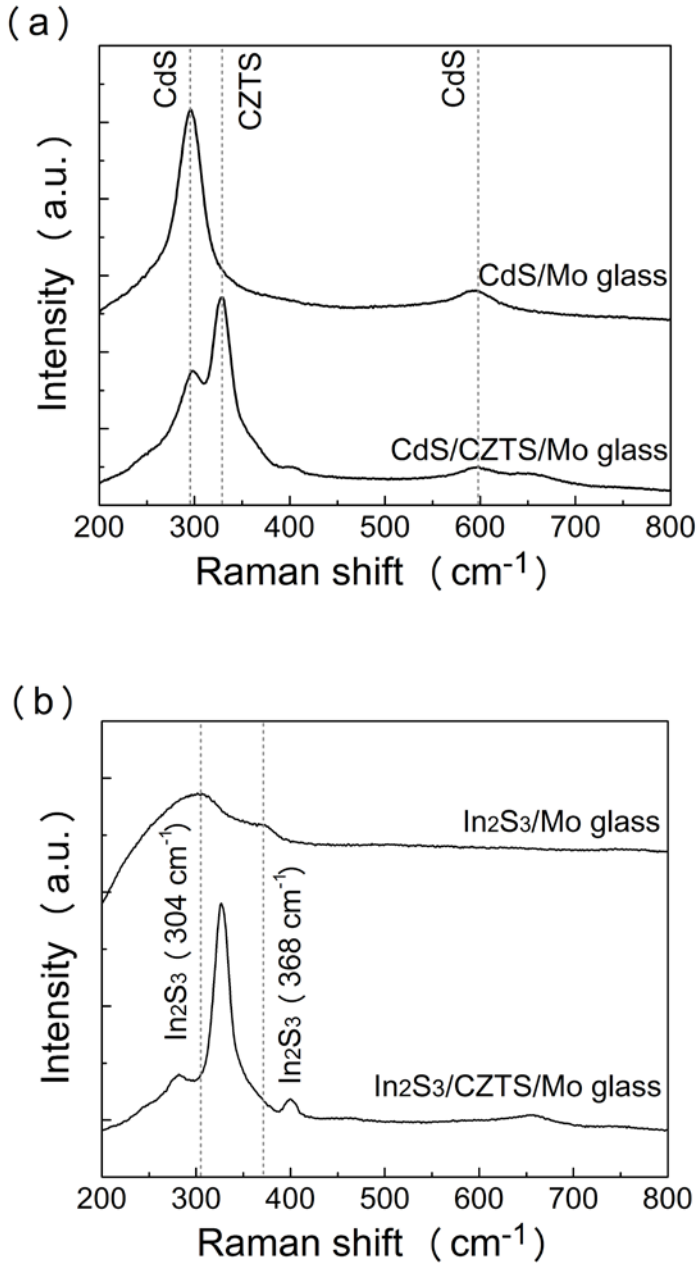

Figure 5. Raman spectra for (a) CdS/Mo glass and CdS/CZTS/Mo glass, (b) In_2S_3/Mo glass and In_2S_3/CZTS/Mo glass.

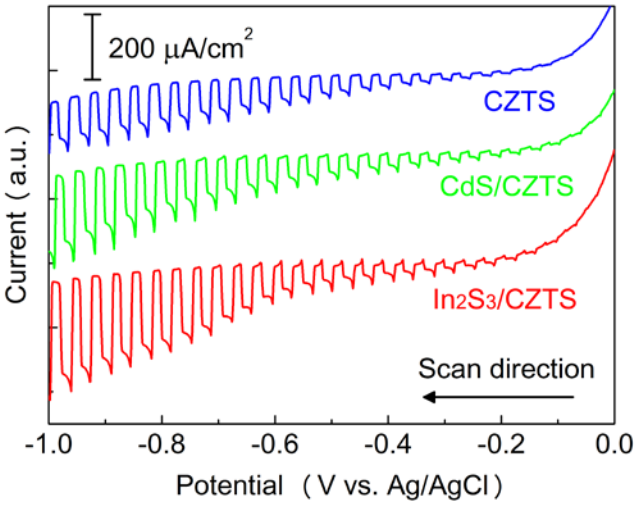

Figure 6. Current−potential curves in 0.1 M NaHCO3 solution under chopped visible light irradiation ($400 < \lambda < 800$ nm, 100 mW/cm^2) for CZTS, CdS/CZTS and In_2S_3/CZTS electrode.

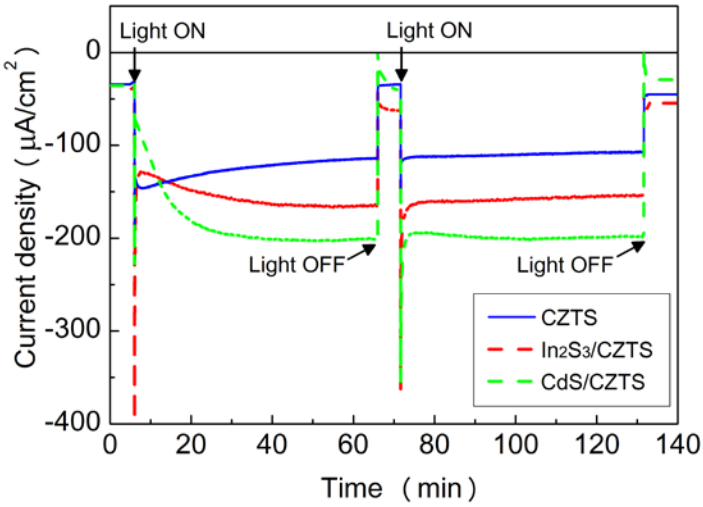

Figure 7. Time course for the photocurrent of CZTS, CdS/CZTS and In2S3/CZTS electrode in aqueous 0.1 M NaHCO3 solution at -1.0 V vs. Ag/AgCl under visible light irradiation ($400 < \lambda <$ 800 nm, 100 mW/cm2).

Table. 1 Photoelectrochemical CO_2 reduction by using CZTS electrode.*

Entry	Sample	Condition	Coulomb (C)	Products						Total (%)
		Purge Gas-Electrolyte		H_2 (μmol)	F. E. for H_2 (%)	CO (nmol)	F. E. for CO(%)	HCOOH (nmol)	F. E. for HCOOH (%)	
1	CZTS	CO_2-$NaHCO_3$	0.8	3.0	72	59	1.4	110	2.7	76.1
2	CZTS	Ar-Na_2SO_4	0.4	1.3	63	n.d.	0	n.d.	0	63.0
3	CdS/CZTS	CO_2-$NaHCO_3$	1.2	5.0	80	435	7.0	75	1.2	88.2
4	In_2S_3/CZTS	CO_2-$NaHCO_3$	1.1	4.1	72	194	3.4	266	4.7	80.1
5	Pt/CdS/CZTS	CO_2-$NaHCO_3$	6.9	20	56	trace	-	trace	-	56.0
6	Pt/In_2S_3/CZTS	CO_2-$NaHCO_3$	5.8	23	77	trace	-	trace	-	77.0

*Visible light irradiation ($400 < \lambda < 800$ nm, 100 mW/cm^2) for 1 h. Applied potential was -1.0 V 381 vs. Ag/AgCl.